

Landau-Lifshitz-Bloch equation for domain wall motion in antiferromagnets

Z. Y. Chen,¹ Z. R. Yan,¹ M. H. Qin,^{1,*} and J.-M. Liu^{1,2}

¹*Institute for Advanced Materials, South China Academy of Advanced Optoelectronics and Guangdong Provincial Key Laboratory of Quantum Engineering and Quantum Materials, South China Normal University, Guangzhou 510006, China*

²*Laboratory of Solid State Microstructures and Innovative Center for Advanced Microstructures, Nanjing University, Nanjing 210093, China*



(Received 6 February 2019; revised manuscript received 6 June 2019; published 25 June 2019)

In this work, we derive the Landau-Lifshitz-Bloch equation accounting for the multidomain antiferromagnetic (AFM) lattice at finite temperature, in order to investigate the domain wall motion, the core issue for AFM spintronics. The continuity equation of the staggered magnetization is obtained using the continuum approximation, allowing an analytical calculation of the domain wall dynamics. The influence of temperature on the static domain wall profile is investigated, and the analytical calculations agree well with the numerical simulations on temperature-gradient-driven domain wall motion, confirming the validity of this theory. Furthermore, the decrease of the acceleration and the increase of the saturation velocity of the domain wall with the increase of temperature are uncovered for a fixed gradient. Moreover, it is worth noting that this theory could be also applied to dynamics of various wall motions in an AFM system. The present theory represents a comprehensive approach to the domain wall dynamics in AFM materials, a crucial step toward the development of AFM spintronics.

DOI: [10.1103/PhysRevB.99.214436](https://doi.org/10.1103/PhysRevB.99.214436)

I. INTRODUCTION

As promising materials for spintronics, antiferromagnets have attracted significant attention recently because they show fast magnetic dynamics and produce nonperturbing stray fields [1–3], especially after the effective detection and manipulation of antiferromagnetic (AFM) state were experimentally realized [4–6]. Theoretically, the spin dynamics in an AFM lattice can also be investigated using the Landau-Lifshitz-Gilbert (LLG) equation based on the atomistic spin models, and a number of driving mechanisms [7–16] have been proposed to drive effectively the domain wall (DW) in an AFM lattice. These important works not only contribute a great deal to fundamental physics but also do provide useful information for potential AFM spintronic devices.

Nevertheless, for a realistic spintronic device where the lattice size under consideration is huge, atomistic spin models are far from sufficient and an efficient computation based on such atomistic models becomes nonrealistic due to the computation capacity limit. Considering that an AFM DW may have a spatial width as large as ~ 10 nm, one sees that the whole lattice used for the LLG-based micromagnetic simulation must be at least as large as ~ 100 nm if wall motion is considered. This makes a computation impossible due to the capacity limit, unless the lattice is cut down to ~ 10 nm. At a cost of physical reality, one has to set the axial anisotropies two orders of magnitude stronger than realistic values, and the DW becomes unreasonably narrow (~ 1 nm). Moreover, white-noise terms are usually included into the effective field for the LLG dynamics in order to simulate temperature (T)-dependent effects, which also add huge computation cost to the simulations.

As an alternative approximation, one may utilize the coarse-grained scheme and use a macromoment $\mathbf{m}_v/\mathbf{m}_k$ to express the two sublattice magnetizations of a finite region (called a grain) inside a AFM domain, and thus the LLG equation on the macromoment $\mathbf{m}_v/\mathbf{m}_k$ can be used without increasing the computational cost much. However, the LLG-based simulations fail to capture the fact that the magnetization magnitude is a function of T : usually it decreases with increasing T until the transition point T_N . Thus, the AFM DW dynamics at finite T especially near T_N is hardly described by the LLG simulations. Furthermore, the same problem also exists in the derivation of the micromagnetic continuum equations for staggered magnetization from the LLG equation based on the coarse-grained scheme. Realistic appealing to numerical approaches is thus raised in order to treat the wall dynamics in an AFM system at finite T or T gradient, noting that the T -relevant controls, e.g., T -gradient-driven wall motions have been often taken in the AFM spintronic devices.

In short, there is an urgent need to develop an approach in dealing with discrete and continuum models for AFM lattice at elevated T . Compared to the LLG equation, the Landau-Lifshitz-Bloch (LLB) equation introduces the longitudinal relaxation to describe the T -dependent magnitude of the magnetization, making it possible to reasonably investigate the DW dynamics at finite T even near T_N . As a matter of fact, it is noted that wall motion in a FM lattice under a T -gradient field has been simulated using the LLB equation [17,18]. This computation has been proven to be efficient in large-scale micromagnetic simulation of realistic spintronic devices at high T and in short time. Reasonable results on the wall motion and Walker breakdown in a multidomain FM lattice have been obtained within the framework of the LLB equation. Most recently, the results on the multidomain FM lattice suggested a linear relation between the wall velocity and T gradient. This relation was once applied to describe the domain wall

*qinmh@scnu.edu.cn

motion in an AFM lattice. Unfortunately, this relation agrees with numerical results under small T gradient, but deviates seriously when the T gradient is large [14]. It is inconsistent with the fact that the wall velocity should be limited by the maximum spin-wave group velocity [9,10]. We would thus be highly concerned and interested to ask if the LLB scheme can be applied to track efficiently the domain wall motion in a large and multidomain AFM lattice. Indeed, the LLB equation on a ferrimagnetic monodomain lattice was recently proposed [19,20], which becomes the basis for deriving a generalized equation for a multidomain AFM lattice.

In this work, we perform a derivation of the LLB equation for a multidomain AFM lattice at finite T ; this equation would be highly efficient for large-scale micromagnetic simulation of realistic AFM spintronic devices. More importantly, a continuity equation for the staggered magnetizations can be derived from this equation using the continuum approximation, which allows an analytical calculation on the domain wall motion in an AFM lattice (e.g., driven by a finite T gradient or staggered magnetic field). It is found that the theory's predictions about several crucial issues agree well with numerical results in literature.

II. DERIVATION OF THE LLB EQUATION

We start from an AFM lattice with two intercrossing FM sublattices whose spin alignments are antiparallel. We apply the coarse-grained scheme to the whole lattice divided into a number of grains as shown in Fig. 1. The grain size should be sufficiently large for high-efficiency computation but sufficiently small in comparison with the concerned characteristic scales in lattice, e.g., domain wall width or other anomalies in the present case. The basic strategy is to track the magnetization evolution of the two sublattices separately, which makes it possible to investigate the AFM dynamics using a method similar to that of ferromagnets [21,22]. For an arbitrary grain (i) containing two FM sublattices (v, κ), if no interaction of this grain with its neighbors is considered, the LLB equation for magnetization \mathbf{m}_v of sublattice v is written as [19]

$$\frac{1}{\gamma_v} \frac{d\mathbf{m}_v}{dt} = \mathbf{m}_v \times \mathbf{H}_v + \alpha_{\parallel} \frac{\mathbf{m}_v \cdot \mathbf{H}_v}{m_v^2} \mathbf{m}_v - \alpha_{\perp} \frac{\mathbf{m}_v \times (\mathbf{m}_v \times \mathbf{H}_v)}{m_v^2}, \quad (1)$$

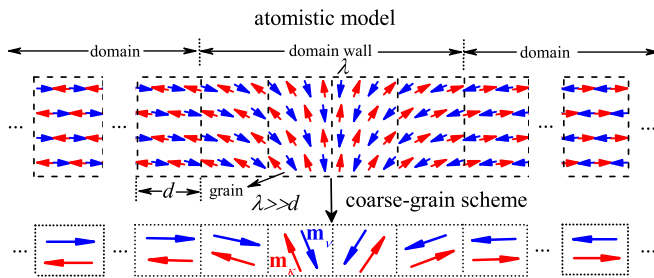


FIG. 1. (Top) Spin configuration of atomistic regular AFM lattice, where the whole AFM lattice is divided into many grains (regions). (Bottom) Sublattice magnetization in a grain is described by two antiparallel macrospins \mathbf{m}_v and \mathbf{m}_κ .

where γ_v is the gyromagnetic ratio, $\alpha_{\parallel}/\alpha_{\perp}$ are the T -dependent longitudinal/transverse damping constants, $\mathbf{H}_v = \mathbf{H} + \mathbf{H}_{A,v} + \mathbf{H}_{v\kappa}$ is the effective field including external field \mathbf{H} , anisotropy field $\mathbf{H}_{A,v}$ and internal exchange field $\mathbf{H}_{v\kappa}$, assuming the z axis as the easy axis. The internal exchange field $\mathbf{H}_{v\kappa}$ accounts for the interaction between the sublattices v and κ . They are, respectively, given by [19]

$$\mathbf{H}_{A,v} = -\frac{1}{\tilde{\chi}_{v,\perp}} (m_{x,v} \mathbf{e}_x + m_{y,v} \mathbf{e}_y),$$

$$\mathbf{m}_v = (m_{x,v} \mathbf{e}_x, m_{y,v} \mathbf{e}_y, m_{z,v} \mathbf{e}_z), \quad (2)$$

and

$$\mathbf{H}_{v\kappa} = -\frac{J_{0,v\kappa}}{\mu_v} \frac{\mathbf{m}_v \times (\mathbf{m}_v \times \mathbf{m}_\kappa)}{m_v^2} - \frac{1}{2} \left[\frac{1}{\Lambda_{vv}} \left(\frac{m_v^2}{m_{e,v}^2} - 1 \right) - \frac{1}{\Lambda_{v\kappa}} \left(\frac{\tau_\kappa^2}{\tau_{e,\kappa}^2} - 1 \right) \right] \mathbf{m}_v, \quad (3)$$

where $\chi_{v,\perp}$ is the transverse susceptibility, $J_{0,v\kappa}$ is the coupling constant, μ_v is the saturation moment, $m_{e,v}$ is the equilibrium magnetization, Λ_{vv} and $\Lambda_{v\kappa}$ are the longitudinal rates, $\tau_\kappa = \mathbf{m}_v (\mathbf{m}_v \cdot \mathbf{m}_\kappa) / m_v^2$, and $\tau_{e,\kappa} = |\mathbf{m}_{e,v} \cdot \mathbf{m}_{e,\kappa}| / m_{e,v}$ [19]. The first and third terms on the right side of Eq. (1) have the same forms as those in the LLG equation, and the second term describes the longitudinal relaxation depicting the magnitude variation of magnetization due to thermal fluctuations at finite T .

It is noted that the T -dependent parameters in the two sublattices equal each other (e.g., $\gamma_v = \gamma_\kappa = \gamma$, $m_{e,v} = m_{e,\kappa} = m_e$, $\mu_v = \mu_\kappa = \mu_S$, $\chi_{v,\perp} = \chi_{\kappa,\perp} = \chi_{\perp}$), and $\mathbf{H}_{v\kappa}$ has a more compact form:

$$\mathbf{H}_{v\kappa} = -\frac{J_0}{\mu_S} \frac{\mathbf{m}_v \times (\mathbf{m}_v \times \mathbf{m}_\kappa)}{m_v^2} - \frac{1}{2} \left[\frac{1}{\tilde{\chi}_{\parallel}} \left(\frac{m_v^2}{m_e^2} - 1 \right) + \frac{|J_0|}{\mu_S} \frac{m_v^2 - \tau_\kappa^2}{m_e^2} \right] \mathbf{m}_v, \quad (4)$$

where χ_{\parallel} is the longitudinal susceptibility, $J_{0,v\kappa} = J_0 = N_D J$, where J is the exchange coupling between the nearest-neighbor atomistic spins and N_D is the coordination number. Following the earlier works [21–23], these parameters m_e , χ_{\parallel} , and χ_{\perp} are reasonably estimated by numerical simulations using the stochastic LLG equation based on the atomistic model. As an example, we present the estimated parameters (empty points) and corresponding fitted results (solid lines) in Fig. 2, given the uniaxial anisotropy $0.02J$. Their good consistencies confirm the estimations.

Subsequently, we discuss the effect of T . It is noted that thermal fluctuations are less dependent on spin structures, and thus the stochastic fields for a FM system can be approximately applicable to an AFM system [24–26]. This argument has been confirmed in earlier work which calculates the stochastic fields strictly using the Fokker-Planck equation [23]. When the stochastic fields are considered, the LLB

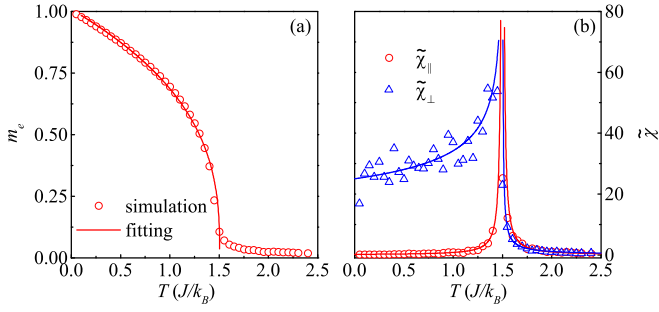


FIG. 2. Stochastic LLG simulated (a) m_e and (b) χ_{\parallel} and χ_{\perp} as functions of temperature and the corresponding fitting results.

equation for grain (i) now reads

$$\frac{1}{\gamma} \frac{d\mathbf{m}_v}{dt} = \mathbf{m}_v \times \mathbf{H}_v + \alpha_{\parallel} \frac{\mathbf{m}_v \cdot \mathbf{H}_v}{m_v^2} \mathbf{m}_v - \alpha_{\perp} \frac{\mathbf{m}_v \times [\mathbf{m}_v \times (\mathbf{H}_v + \xi_{\perp,v})]}{m_v^2} + \xi_{\parallel,v} \quad (5)$$

where $\xi_{\parallel,v}/\xi_{\perp,v}$ is the longitudinal/transverse stochastic field with

$$\langle \xi_{\eta,v}^a(t, \mathbf{r}) \xi_{\eta,v}^b(t', \mathbf{r}') \rangle = 2D_{\eta} \delta_{ab} \delta(t - t') \delta(\mathbf{r} - \mathbf{r}'), \quad \eta = (\parallel, \perp), \quad (6)$$

where a, b are the Cartesian components ($= x, y, z$), and the longitudinal and transverse diffusion constants D_{\parallel} and D_{\perp} read, respectively,

$$D_{\parallel} = \frac{\alpha_{\parallel} \gamma k_B T}{M_S V}, \quad \text{and} \quad D_{\perp} = \frac{(\alpha_{\perp} - \alpha_{\parallel}) k_B T}{\gamma M_S V \alpha_{\perp}^2} \quad (7)$$

where k_B is the Boltzmann constant, M_S the saturation magnetization, and V the grain volume.

It is noted that in order to describe thermal fluctuations and satisfy the fluctuation-dissipation theorem, fluctuating torques and fluctuating fields are introduced into the damping term of the LLB equation. Alternatively, fluctuating fields are introduced into the precession and damping terms of the LLG equation. As a result, the LLG equation cannot be completely recovered from the LLB equation in the absence of the longitudinal dynamics. Moreover, the calculations based on the stochastic LLB equation and stochastic LLG equation are expected to be consistent with each other at low T far below the Néel temperature (T_N). However, the thermal effects at rather high T cannot be well investigated based on the stochastic LLG equation because it fails to capture the T -dependent magnetization magnitude.

Actually, any grain must have coupling with its neighbors and an inclusion of the coupling is a prerequisite to consider a multidomain AFM system. We discuss the intergrain exchange field between grain (i) and grain (j), using the same approach as given in Ref. [22] to extend the LLB equation. For two neighboring grains (i) and (j), the intergrain exchange

interaction H_{exij} reads

$$H_{exij} = -J \sum_{\langle k,l \rangle} \mathbf{S}_k \cdot \mathbf{S}_l = -J \frac{F}{2a_l^2} \left(\frac{\mathbf{m}_{v,i}}{m_{v,i}} \cdot \frac{\mathbf{m}_{\kappa,j}}{m_{\kappa,j}} + \frac{\mathbf{m}_{\kappa,i}}{m_{\kappa,i}} \cdot \frac{\mathbf{m}_{v,j}}{m_{v,j}} \right), \quad (8)$$

where $\langle k, l \rangle$ sums all the nearest-neighbor pairs connecting the two grains, \mathbf{S} is the normalized atomistic spin, F is the interface area, and a_l is the lattice constant, $\mathbf{m}_{v,i}/m_{\kappa,j}$ is the magnetization of sublattice v/κ in grain i/j . Then, we obtain the intergrain exchange field to sublattice v of grain (i) imposed by sublattice κ in grain (j):

$$\mathbf{H}_{ex,v,i} = -\frac{1}{M_S V/2} \frac{\partial H_{exij}}{\partial \mathbf{m}_{v,i}} = \frac{2A(0)}{a_l d M_S m_e^2} (\mathbf{m}_{\kappa,j} + \mathbf{m}_{v,i}), \quad (9)$$

where $A(0) = J/2a_l$ is the exchange stiffness at zero T , and d is the grain dimension. It is noted that Eq. (9) is obtained on the assumption that the two sublattices' magnetizations in grains (i) and (j) can be described as macrospins $\mathbf{m}_{v,i}$ and $\mathbf{m}_{\kappa,j}$. This would overestimate the intergrain exchange coupling. Following the earlier work, a correction factor a_l/d should be taken into account to diminish the overestimation [22].

Moreover, considering the thermal fluctuations, the exchange stiffness is also T dependent, given by $A(T) = A(0)m_e^2$ if the thermal average spin moment is equal to the equilibrium magnetization m_e . Thus, the total intergrain exchange field of sublattice v in grain i reads

$$\mathbf{H}_{ex,v,i} = \frac{2A(T)}{d^2 M_S m_e^2} \sum_j (\mathbf{m}_{\kappa,j} + \mathbf{m}_{v,i}), \quad (10)$$

where the sum is over all the nearest-neighboring grains.

To this stage, we have successfully obtained the LLB equation applicable to a multidomain AFM lattice, in particular, to describe the domain wall dynamics. Certainly, a more explicit form of the LLB equation using the continuum approximation would be appreciated [16]. In proceeding, we define the total magnetization $\mathbf{m}_i = \mathbf{m}_{v,i} + \mathbf{m}_{\kappa,i}$ and staggered magnetization $\mathbf{n}_i = \mathbf{m}_{v,i} - \mathbf{m}_{\kappa,i}$ for grain (i) to replace $\mathbf{m}_{v,i}$ and $\mathbf{m}_{\kappa,i}$. The effective fields for grains (i) and (j) are then written as $\mathbf{H}_{v,i} = \mathbf{H}_{m,i} + \mathbf{H}_{n,i}$, and $\mathbf{H}_{\kappa,i} = \mathbf{H}_{m,i} - \mathbf{H}_{n,i}$, where $\mathbf{H}_{m,i}$ and $\mathbf{H}_{n,i}$ are, respectively, the effective fields related to \mathbf{m}_i and \mathbf{n}_i . Noting that the longitudinal relaxation of sublattice magnetization is much faster than the transverse relaxation, and the magnetization is nearly identical to the equilibrium one, i.e., $|\mathbf{m}_{v,i}| = m_{e,i}$ [18,19], one has the alternative expressions of the LLB equations after necessary substitutions and continuum approximation:

$$\frac{d\mathbf{m}}{dt} = \gamma (\mathbf{m} \times \mathbf{H}_m + \mathbf{n} \times \mathbf{H}_n) - \frac{\alpha_{\perp}}{2m_e^2} \left(\mathbf{m} \times \frac{d\mathbf{m}}{dt} + \mathbf{n} \times \frac{d\mathbf{n}}{dt} \right) + \frac{\gamma \alpha_{\parallel}}{2m_e^2} [(\mathbf{m} \cdot \mathbf{H}_n) \mathbf{n} + (\mathbf{n} \cdot \mathbf{H}_m) \mathbf{n}], \quad (11)$$

and

$$\frac{d\mathbf{n}}{dt} = \gamma \mathbf{n} \times \mathbf{H}_m, \quad (12)$$

with the effective fields \mathbf{H}_m and \mathbf{H}_n (see Ref. [27] for detailed derivation). Here, Eq. (11) has been transformed into the Gilbert form, and particular damping terms are safely omitted as done in the LLG scheme [16,28,29], which hardly affects our main results.

For an AFM system below T_N , one has $\mathbf{m} \cdot \mathbf{n} \sim 0$, and $\mathbf{n}^2 \sim 4m_e^2$ which is also T dependent due to the fact that the longitudinal relaxation is generally much faster than the transverse one. Under zero applied field, \mathbf{m} as a function of \mathbf{n} can be derived from Eq. (12) [16,29]:

$$\mathbf{m} = \frac{\frac{d\mathbf{n}}{dt} \times \mathbf{n}}{4\gamma m_e^2 (J_0/\mu_S + 2N_D A/d^2 M_S m_e^2)} = A_m \frac{d\mathbf{n}}{dt} \times \mathbf{n}, \quad (13)$$

where parameter A_m is introduced for brevity. Substituting Eq. (13) into Eq. (11) and taking the cross product with \mathbf{n} , we obtain

$$A_m \mathbf{n} \times \frac{d^2 \mathbf{n}}{dt^2} \times \mathbf{n} = \mathbf{n} \times \left(-\frac{\gamma}{2\tilde{\chi}_\perp} n_z \mathbf{e}_z + \frac{\gamma A(T)}{M_S m_e^2} \nabla^2 \mathbf{n} + \frac{\alpha_\perp}{2m_e^2} \frac{d\mathbf{n}}{dt} \right) \times \mathbf{n}, \quad (14)$$

where n_z is the z component of \mathbf{n} . Specifically, all parameters including exchange, magnetic anisotropy, and damping parameters are T dependent in Eq. (14). More importantly, the magnitude of \mathbf{n} also depends on T by introducing the longitudinal relaxation, which is basically different from the equation derived from the LLG equation. We have obtained an analytical expression of the staggered magnetization for an AFM lattice, whose magnitude and orientation are spatially inhomogeneous and T dependent. It thus allows one to track various stimuli-driven domain structure evolution and wall motion in a multidomain AFM system.

By using Eqs. (13) and (14), we can perform the analytical calculations within the framework of the LLB equation for an AFM system. Here, the second-order derivative of \mathbf{n} with respect to time is essential in distinguishing the magnetic dynamics in an AFM system from that in a FM one [30]. In particular, the parameters and magnitude for the staggered magnetization (\mathbf{n}) are T dependent, allowing one to investigate the magnetic dynamics at finite T , including the domain wall motion in ultralarge scale. Furthermore, the domain wall motion in an AFM lattice, as driven by various stimuli such as temperature gradient [13–15], external field [28,31,32], and Néel spin-orbit torque [10,33], can be similarly calculated using Eq. (14).

III. APPLICATION OF THE LLB EQUATION

For the validity of this continuum LLB theory on AFM lattice, one looks to several well-known facts for checking. As an initial check, we discuss the static solutions. One of the special solutions to Eq. (14) is the static Néel wall configuration with the polar angle of the staggered magnetization $\theta = 2\arctan[\exp(z - z_0)/\lambda]$, where z_0 is the position of the wall center, and λ is the T -dependent wall width:

$$\lambda(T) = \sqrt{\frac{2\tilde{\chi}_\perp |A(T)|}{M_S m_e^2}}. \quad (15)$$

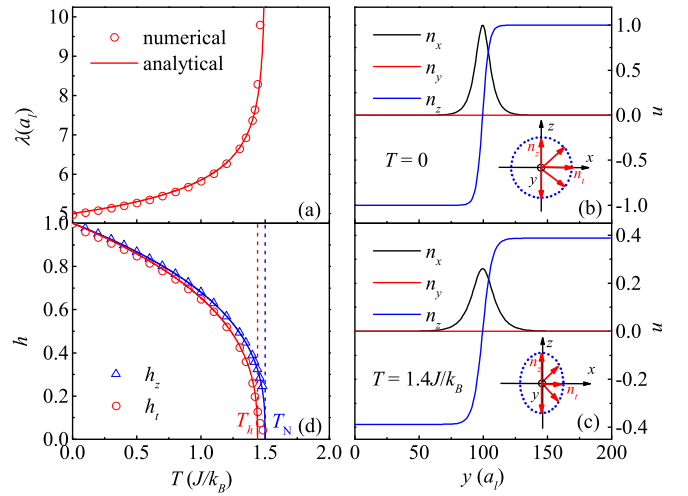


FIG. 3. (a) Numerical and analytical calculated λ as a function of T , and the three components of the magnetization versus y coordinate at (b) $T = 0$ and (c) $T = 1.4 J/k_B$, and (d) the estimated h_z and h_t as functions of T . The sketches of circular and elliptical DWs are also presented, respectively, in the insets of (b) and (c).

One observes that $\lambda(0)$ is exactly the same as that derived from the LLG equation [16]. Moreover, λ increases with increasing T and ultimately becomes divergent at T_N , as shown in Fig. 3(a), which gives the numerical and analytical calculated λ as a function of T . The analytical data well coincide with the numerical results, both based on the LLB equation, supporting the validity of this continuum theory.

It is noted that the AFM DW profiles have important influence on the wall dynamics and relevant magnetoresistance, while their T dependences are still unclear so far. We numerically study the effect of temperature on the Bloch DW profiles using Eq. (5) on an $8a_l \times 8a_l \times 200a_l$ system. Similar to ferromagnets [34–36], three types of walls including circular, elliptical, and linear walls are observed. The circular wall emerges at zero T , as shown in Fig. 3(b) which gives the three components of the magnetization versus y coordinate. Figure 3(c) presents the components at $T = 1.4 J/k_B$, which clearly demonstrates an elliptical wall. Similarly, the wall profiles can be described by the hyperbolic functions $n_z(T) = h_z(T) \tanh[(y - y_0)/\lambda(T)]$ and $n_t(T) = h_t(T) \text{sech}[(y - y_0)/\lambda(T)]$, where n_t is the transverse component of \mathbf{n} , and h_z/h_t is the amplitude of easy axis/transverse magnetization. The estimated $h_z(T)$ and $h_t(T)$ are summarized in Fig. 3(d) where h_t is smaller than h_z at finite T , demonstrating the existence of elliptical walls. In addition, for $T_h < T < T_N$, the domain wall is linear with a finite h_z and zero h_t . This effect can be understood from the influence of thermal fluctuations on the DW. The spins in the wall usually deviate from the easy axis and have large exchange and anisotropy energies, and thus they are more sensitive to thermal fluctuations than the spins inside the domain, resulting in the fact that h_t decreases more quickly than h_z as T increases, as confirmed in our simulations. Furthermore, the difference between $h_z(T)$ and $h_t(T)$ increases with the increasing anisotropy (the corresponding results are not shown here), the same as in FM systems [34,35]. As a

matter of fact, earlier work claimed that the FM and AFM domain walls share common static properties at zero T [37]. Here, it is clearly demonstrated that this behavior also exists at finite T even near T_N .

Given the validity of the developed LLB theory, we intend to solve Eq. (14) using the approach with polar coordinates proposed in earlier work to investigate the thermally driven DW motion for an AFM lattice in a finite T gradient [10,38]. As has been clarified in the earlier works [13–15], the competition between the entropy torque and Brownian force under a T gradient determines the motion of AFM DW. Here, we pay particular attention on the entropy torque-driven DW motion where the stochastic field can be safely neglected. Furthermore, we assume that T is rather below T_N and the DW structure is robust during its motion [9,38–40]. In this case, the staggered magnetization is a function of the composite variable $Z = z - vt$:

$$\frac{dn_x}{dt} = -vn'_x, \quad \frac{dn_z}{dt} = -vn'_z, \quad \frac{d\theta}{dt} = -v\theta' = -v \frac{\sin \theta}{\lambda}, \quad (16)$$

where v is the wall velocity, θ is the angle between the staggered magnetization and z axis, and the prime represents the derivative with respect to Z . We obtain the velocity of wall motion under a temperature gradient:

$$v = \frac{-\frac{1}{\alpha_1} + \sqrt{\frac{1}{\alpha_1^2} + 4\alpha_2}}{2\alpha_2}, \quad (17)$$

where α_1 and α_2 are T -dependent variables (see Ref. [27] for details). One may note that an anisotropy gradient could be induced by the T gradient [see the $\chi_\perp(T)$ curve in Fig. 2(b)], which also contributes to the DW motion [41,42]. However, comparing with the effect of the strong exchange interaction, the effect of the anisotropy term on the DW dynamics can be safely ignored. More interestingly, it is also demonstrated that the DW velocity is limited by

$$v_{\max} = \frac{\gamma a_l J \sqrt{2N_D}}{\mu_S} m_e = c(T), \quad (18)$$

where $c(0)$ is the group velocity of spin wave at zero T (see Ref. [27] for details), further confirming the fact that the limitation of the DW velocity originates from the emission of spin wave [9,16]. With the increasing T , the enhanced thermal fluctuations effectively weaken the exchange interaction and in turn suppress $c(T)$ and v_{\max} . In Fig. 4(a), the LLG simulated, the LLB simulated, and analytically calculated velocities are presented, and the good coincidence of these results confirms the validity of the effective theory. Interestingly, ~ 1000 CPU hours are needed for the LLG simulations performed on our computer cluster, while only ~ 2 CPU hours are needed for the LLB simulations, demonstrating the high efficiency of the theory in dealing with the antiferromagnetic dynamics.

More importantly, one may perform the LLB simulations to investigate the AFM dynamics at high temperatures even near T_N . In Fig. 4(b), the LLB-simulated DW positions as functions of t under $\nabla T = 0.003 J/k_B a_l$ for various T_0 (the lowest temperature of the system) are presented, which demonstrates the difference of the DW dynamics for high T_0 from low T_0 . On the one hand, the DW quickly accelerates

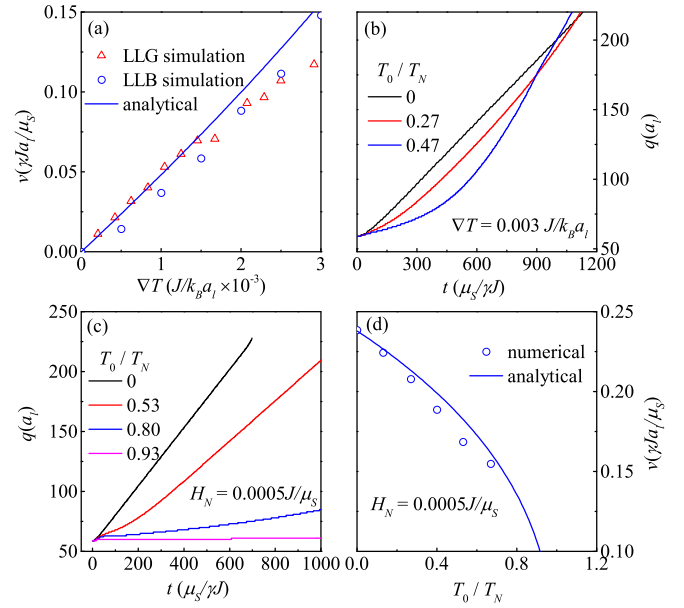


FIG. 4. LLG-simulated (empty triangles), the LLB-simulated (empty circles), and analytically (solid line) calculated DW velocities as functions of ∇T (a), and the LLB-simulated DW positions as functions of t for various T_0 (b) under $\nabla T = 0.003 J/k_B a_l$, and (c) under the effective staggered field $H_N = 0.0005 J/\mu_S$, and (d) the LLB simulated (empty circles) and analytically calculated (solid line) velocities as functions of T_0 under $H_N = 0.0005 J/\mu_S$. The LLG simulated results in (a) are reproduced from Ref. [14].

to the saturation velocity for low T_0 , and the accelerating time significantly increases with the increase of T_0 , as clearly shown in the movies in the Supplemental Material [27]. It is noted that the exchange interaction between neighboring spins is effectively reduced as T_0 increases, contributing to the decrease of the acceleration. On the other hand, higher T_0 generally results in stronger changes of the magnetization and driving torque, resulting in a larger saturation velocity, as shown in the simulations.

In order to better understand the temperature effect on the DW dynamics, we also investigated the DW motion driven by an effective staggered field H_N along the z axis (H_N and $-H_N$ are applied on v and κ sublattices, respectively), which could be induced by electric current in CuMnAs and Mn₂Au. The LLB-simulated DW positions as functions of t for various T_0 are shown in Fig. 4(c), which clearly shows that both the acceleration and saturation velocity are significantly suppressed with the increase of T_0 , attributed to the reduction of the effective exchange interaction. Similarly, the velocity of wall motion under the staggered field could be also analytically calculated:

$$v_N = \frac{\lambda H_N}{\alpha_\perp} m_e. \quad (19)$$

Figure 4(d) gives the LLB-simulated and analytically calculated DW velocities. The results for $T_0 < 2T_N/3$ well coincide with each other, while deviating from each other for $T_0 > 2T_N/3$. It is noted that the divergence of the longitudinal relaxation time at $T \sim T_N$ is hardly captured by the approximate condition $\mathbf{n}^2 \sim 4m_e^2$, resulting in the deviation of the

analytical results from the numerical results. However, the physics has been clearly uncovered by the LLB simulations, and the investigation is far beyond the capacity of the present LLG method, which fails to describe the temperature dependence of the magnetization magnitude.

IV. DISCUSSION AND CONCLUSION

So far, the validity of the dynamic equation for staggered magnetization in an AFM lattice has been well confirmed by checking the static domain wall profiles and T -gradient-driven wall motion which are well consistent with the numerical results. Thus, the two major issues (AFM wall motion at finite T in large-scale system) which are hardly reached in the LLG-based simulations have been removed if the LLB equation and derived continuum equation are utilized. More importantly, we would like to point out that this essential equation can be also used to investigate the AFM dynamics driven by other stimuli [43–45]. For example, a large-scale system is needed to generate Gauss T field, which is hardly reached by the conventional LLG simulations [46]. As a matter of fact, the analytical calculation has been performed, and the corresponding results will be reported elsewhere.

In conclusion, we have derived the LLB equation with intergrain and stochastic fields for AFM systems, which

allows one to investigate the magnetic dynamics at finite temperatures using multiscale approaches. Moreover, the continuity equation of the staggered magnetization has been also derived using the continuum approximation. The derivations have been used to investigate the influence of temperature on the static AFM domain wall, which reveals a similar behavior to FM systems. The analytical calculation of the temperature-gradient-driven AFM domain wall motion well agrees with the numerical results and reproduces successfully the saturation velocity, well confirming the validity of our derivations. More interestingly, physics-related DW dynamics under temperature gradient has been predicted by the LLB simulations. Importantly, this theory could be applied to other wall driving mechanisms such as Néel spin-orbit torques and spin-transfer torques as well.

ACKNOWLEDGMENTS

The work is supported by the National Key Projects for Basic Research of China (Grant No. 2015CB921202), the Natural Science Foundation of China (Grant No. 11204091), the Science and Technology Planning Project of Guangzhou in China (Grant No. 201904010019), and the Natural Science Foundation of Guangdong Province (Grant No. 2016A030308019).

-
- [1] O. Gomonay, V. Baltz, A. Brataas, and Y. Tserkovnyak, *Nat. Phys.* **14**, 213 (2018).
- [2] P. Němec, M. Fiebig, T. Kampfrath, and A. V. Kimel, *Nat. Phys.* **14**, 229 (2018).
- [3] N. Thielemann-Kühn, D. Schick, N. Pontius, C. Trabant, R. Mitzner, K. Hollmack, H. Zabel, A. Föhlisch, and C. Schüßler-Langeheine, *Phys. Rev. Lett.* **119**, 197202 (2017).
- [4] I. Fina, X. Martí, D. Yi, J. Liu, J. H. Chu, C. R. Serrao, S. Suresha, A. B. Shick, J. Železný, T. Jungwirth, J. Fontcuberta, and R. Ramesh, *Nat. Commun.* **5**, 4671 (2014).
- [5] P. Wadley, B. Howells, J. Železný, C. Andrews, V. Hills, R. P. Campion, V. Novák, K. Olejník, F. Maccherozzi, S. S. Dhesi, S. Y. Martin, T. Wagner, J. Wunderlich, F. Freimuth, Y. Mokrousov, J. Kuneš, J. S. Chauhan, M. J. Grzybowski, A. W. Rushforth, K. W. Edmonds, B. L. Gallagher, and T. Jungwirth, *Science* **351**, 587 (2016).
- [6] X. Z. Chen, R. Zarzuela, J. Zhang, C. Song, X. F. Zhou, G. Y. Shi, F. Li, H. A. Zhou, W. J. Jiang, F. Pan, and Y. Tserkovnyak, *Phys. Rev. Lett.* **120**, 207204 (2018).
- [7] K. M. D. Hals, Y. Tserkovnyak, and A. Brataas, *Phys. Rev. Lett.* **106**, 107206 (2011).
- [8] A. Qaiumzadeh, L. A. Kristiansen, and A. Brataas, *Phys. Rev. B* **97**, 020402(R) (2018).
- [9] T. Shiino, S.-H. Oh, P. M. Haney, S.-W. Lee, G. Go, B.-G. Park, and K.-J. Lee, *Phys. Rev. Lett.* **117**, 087203 (2016).
- [10] O. Gomonay, T. Jungwirth, and J. Sinova, *Phys. Rev. Lett.* **117**, 017202 (2016).
- [11] E. G. Tveten, A. Qaiumzadeh, and A. Brataas, *Phys. Rev. Lett.* **112**, 147204 (2014).
- [12] S. K. Kim, Y. Tserkovnyak, and O. Tchernyshyov, *Phys. Rev. B* **90**, 104406 (2014).
- [13] S. K. Kim, O. Tchernyshyov, and Y. Tserkovnyak, *Phys. Rev. B* **92**, 020402(R) (2015).
- [14] S. Selzer, U. Atxitia, U. Ritzmann, D. Hinzke, and U. Nowak, *Phys. Rev. Lett.* **117**, 107201 (2016).
- [15] Z. R. Yan, Z. Y. Chen, M. H. Qin, X. B. Lu, X. S. Gao, and J.-M. Liu, *Phys. Rev. B* **97**, 054308 (2018).
- [16] E. G. Tveten, T. Muller, J. Linder, and A. Brataas, *Phys. Rev. B* **93**, 104408 (2016).
- [17] D. Hinzke and U. Nowak, *Phys. Rev. Lett.* **107**, 027205 (2011).
- [18] F. Schlickeiser, U. Ritzmann, D. Hinzke, and U. Nowak, *Phys. Rev. Lett.* **113**, 097201 (2014).
- [19] U. Atxitia, P. Nieves, and O. Chubykalo-Fesenko, *Phys. Rev. B* **86**, 104414 (2012).
- [20] F. Schlickeiser, U. Atxitia, S. Wienholdt, D. Hinzke, O. Chubykalo-Fesenko, and U. Nowak, *Phys. Rev. B* **86**, 214416 (2012).
- [21] N. Kazantseva, D. Hinzke, U. Nowak, R. W. Chantrell, U. Atxitia, and O. Chubykalo-Fesenko, *Phys. Rev. B* **77**, 184428 (2008).
- [22] C. Vogler, C. Abert, F. Bruckner, and D. Suess, *Phys. Rev. B* **90**, 214431 (2014).
- [23] C. Vogler, C. Abert, F. Bruckner, and D. Suess, *arXiv:1804.01724* (2018).
- [24] D. A. Garanin, *Phys. Rev. B* **55**, 3050 (1997).
- [25] D. A. Garanin and O. Chubykalo-Fesenko, *Phys. Rev. B* **70**, 212409 (2004).
- [26] R. F. L. Evans, D. Hinzke, U. Atxitia, U. Nowak, R. W. Chantrell, and O. Chubykalo-Fesenko, *Phys. Rev. B* **85**, 014433 (2012).
- [27] See Supplemental Material at <http://link.aps.org/supplemental/10.1103/PhysRevB.99.214436> for details on the derivation of

- the continuum equation, domain wall motion under a temperature gradient, derivation of group velocity of spin waves, and movies on the motion of domain wall under temperature gradient for $T_0 = 0$ and $T_0 = 0.7 J/k_B$.
- [28] K. M. Pan, L. D. Xing, H. Y. Yuan, and W. W. Wang, *Phys. Rev. B* **97**, 184418 (2018).
- [29] H. V. Gomonyay and V. M. Loktev, *Phys. Rev. B* **81**, 144427 (2010).
- [30] A. V. Kimel, B. A. Ivanov, R. V. Pisarev, P. A. Usachev, A. Kirilyuk, and Th. Rasing, *Nat. Phys.* **5**, 727 (2009).
- [31] O. Gomonyay, M. Kläui, and J. Sinova, *Appl. Phys. Lett.* **109**, 142404 (2016).
- [32] Z. Y. Chen, Z. R. Yan, Y. L. Zhang, M. H. Qin, Z. Fan, X. B. Lu, X. S. Gao, and J.-M. Liu, *New J. Phys.* **20**, 063003 (2018).
- [33] Y. L. Zhang, Z. Y. Chen, Z. R. Yan, D. Y. Chen, Z. Fan, and M. H. Qin, *Appl. Phys. Lett.* **113**, 112403 (2018).
- [34] N. Kazantseva, R. Wieser, and U. Nowak, *Phys. Rev. Lett.* **94**, 037206 (2005).
- [35] D. Hinzke, N. Kazantseva, U. Nowak, O. N. Mryasov, P. Asselin, and R. W. Chantrell, *Phys. Rev. B* **77**, 094407 (2008).
- [36] D. A. Garanin, *Physica A* **172**, 470 (1991).
- [37] N. Papanicolaou, *Phys. Rev. B* **51**, 15062 (1995).
- [38] D. Landau and E. Lifshitz, *Phys. Z. der Sowjetunion* **8**, 153 (1935).
- [39] O. A. Tretiakov, D. Clarke, G.-W. Chern, Y. B. Bazaliy, and O. Tchernyshyov, *Phys. Rev. Lett.* **100**, 127204 (2008).
- [40] E. G. Tveten, A. Qaiumzadeh, O. A. Tretiakov, and A. Brataas, *Phys. Rev. Lett.* **110**, 127208 (2013).
- [41] L. C. Shen, J. Xia, G. P. Zhao, X. C. Zhang, M. Ezawa, O. A. Tretiakov, X. X. Liu, and Y. Zhou, *Phys. Rev. B* **98**, 134448 (2018).
- [42] D. L. Wen, Z. Y. Chen, W. H. Li, M. H. Qin, D. Y. Chen, Z. Fan, M. Zeng, X. B. Lu, X. S. Gao, and J. M. Liu, *arXiv:1905.06695* (2019).
- [43] S. Moretti, V. Raposo, E. Martinez, and L. Lopez-Diaz, *Phys. Rev. B* **95**, 064419 (2017).
- [44] S. K. Kim, D. Hill, and Y. Tserkovnyak, *Phys. Rev. Lett.* **117**, 237201 (2016).
- [45] R. Khoshlahni, A. Qaiumzadeh, A. Bergman, and A. Brataas, *Phys. Rev. B* **99**, 054423 (2019).
- [46] U. Atxitia, D. Hinzke, and U. Nowak, *J. Phys. D: Appl. Phys.* **50**, 033003 (2017).